PCCP

ROYAL SOCIETY OF CHEMISTRY

PAPER

View Article Online
View Journal | View Issue

Cite this: *Phys. Chem. Chem. Phys.*, 2020, **22**, 27600

First-principles study of $CaB_{12}H_{12}$ as a potential solid-state conductor for Ca†

Julius Koettgen, ‡[ab] Christopher J. Bartel,[b] Jimmy-Xuan Shen,[ac] Kristin A. Persson [ac] and Gerbrand Ceder*[ab]

Received 25th August 2020,
Accepted 23rd November 2020

DOI: 10.1039/d0cp04500d

rsc.li/pccp

Calcium dodecahydro-*closo*-dodecaborate, $CaB_{12}H_{12}$, was calculated to have a percolating Ca migration path with low activation barrier (650 meV). The formation of Ca vacancies required for diffusion was calculated to be thermodynamically feasible by substitution of Ca with Al, Bi, or a number of trivalent rare-earth cations.

Advances in battery technologies are necessary for a growing demand in energy storage due to the use of energy from sustainable but fluctuating sources, the electrification of transport, and the expansion of mobile applications. Calcium batteries are a potential alternative to current polymer Li-ion and future solid-state lithium technology[1–4] as Ca is more earth-abundant than Li, and resources like cobalt and nickel that are viewed critically today concerning availability and sustainability may be potentially avoided.

The search for the optimal materials that might enable Ca batteries is still in the early stages. Ponrouch *et al.* reported reversible Ca plating and stripping from a traditional liquid carbonate-based electrolyte at elevated temperature, but the Coulombic efficiency was found to be low.[5] Wang *et al.* showed that Ca can be plated and stripped at room temperature.[6] Lipson *et al.* demonstrated reversible Ca intercalation using manganese hexacyanoferrate (MFCN) as a cathode material, a dry nonaqueous liquid electrolyte, and elemental tin as the anode.[7] Ca metal would be preferred as the anode, but no electrolyte has yet been shown to reversibly plate and strip Ca metal with high Coulombic efficiency.[5,8] In this work, we discuss a possible Ca solid-state electrolyte, which promises superior mechanical and thermal stability to liquid electrolytes, for example as would be implemented in a Ca intercalation battery consisting of a Ca metal anode, a solid electrolyte, and a Ca intercalation cathode. The conductivity may not be high enough for room temperature operation, but at elevated temperature sufficient Ca mobility should exist. However, a solid-state electrolyte requires high Ca mobility to enable sufficient Ca transport at low operating temperatures. For example, for Li and Mg solid-state electrolytes, migration barriers as low as 250 and 370 meV have been reported, respectively,[9–11] and similar migration barriers are required for Ca solid-state electrolytes. However, few materials with low Ca migration barriers and low electronic conductivity are known. β″-alumina may be one of the few materials that has been considered as a high-temperature Ca solid-state electrolyte with an experimental activation energy for Ca conduction of 570 meV[12] but has been mostly considered for high-temperature batteries.[13]

Previously discussed candidates for Mg solid-state electrolytes are materials based on *closo*-borates[14] including $B_{12}H_{12}^{2-}$, $B_{10}H_{10}^{2-}$, $CB_9H_{10}^{-}$, and $CB_{11}H_{12}^{-}$ anions that show high Li and Na conductivities (10^{-1} S cm^{-1}).[15–23] In fact, *closo*-borate salts have been intensively discussed for use in liquid electrolytes for Mg and Ca batteries.[24,25]

In this work, Ca diffusion in calcium dodecahydro-*closo*-dodecaborate, $CaB_{12}H_{12}$, was investigated using *ab initio* calculations to assess its potential as a Ca solid-state electrolyte. Density-functional theory (DFT) calculations combined with the nudged elastic band (NEB) method were used to calculate the minimum energy pathways as well as the migration energies for Ca diffusion. $CaB_{12}H_{12}$ was previously synthesized[26] and characterized theoretically,[27] but has not been previously considered as a potential solid-state Ca conductor. The Li and Na analogs, $Li_2B_{12}H_{12}$, and $Na_2B_{12}H_{12}$, show high ion mobility with low migration barriers of about 0.2 eV in calculations (Li, Na) and 0.45 eV experiments (Li).[23] Here, we show that the percolating Ca migration path has a calculated

[a] *Materials Sciences Division, Lawrence Berkeley National Laboratory, Berkeley, CA 94720, USA. E-mail: gceder@berkeley.edu*
[b] *Department of Materials Science and Engineering, University of California, Berkeley, CA 94720, USA*
[c] *Energy Technologies Area, Lawrence Berkeley National Laboratory, Berkeley, CA, USA*

† Electronic supplementary information (ESI) available: Description of the computational methods. See DOI: 10.1039/d0cp04500d

‡ Present address: Volkswagen AG, Volkswagen Group Components, Salzgitter, Germany.

activation barrier of 0.65 eV by a vacancy-mediated diffusion mechanism.

The crystal structure of $CaB_{12}H_{12}$ is shown in Fig. 1. Ca^{2+} ions are surrounded by five icosahedral $[B_{12}H_{12}]^{2-}$ anions and interact with eight neighboring H atoms.[26] Three of the $[B_{12}H_{12}]^{2-}$ anions form a triangular equatorial plane that is centered on each Ca^{2+} ion. Two of the $[B_{12}H_{12}]^{2-}$ anions are in axial position. In $CaB_{12}H_{12}$, there are five geometrically unique Ca migration paths with a migration path length less than 9 Å (Fig. 1 and Fig. S1, see ESI†). Three Ca migration paths connect Ca sites that are in different layers of the $B_{12}H_{12}$-cages. Two Ca migration paths connect Ca sites that are in the same layer of the $B_{12}H_{12}$-cages. Our calculations show that migration between the layers occurs with a smaller activation barrier than migration in the layers. Fig. 2 shows the calculated energies relative to the initial state along the migration paths. In the $B_{12}H_{12}$ layers, Ca migration barriers vary between 1300–1400 meV.

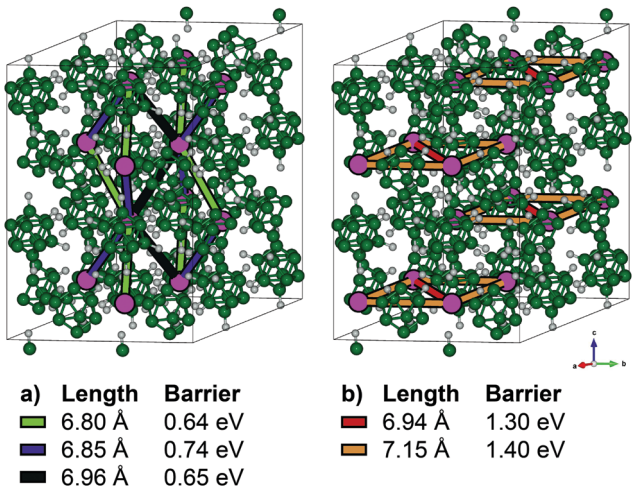

Fig. 1 $CaB_{12}H_{12}$ structure and possible migration paths. Ca is shown as pink spheres, B as green spheres, and H as grey spheres. Possible migration paths below 9 Å are shown as lines between Ca positions. (a) Paths between layers have lower migration barriers than (b) paths within the layers.

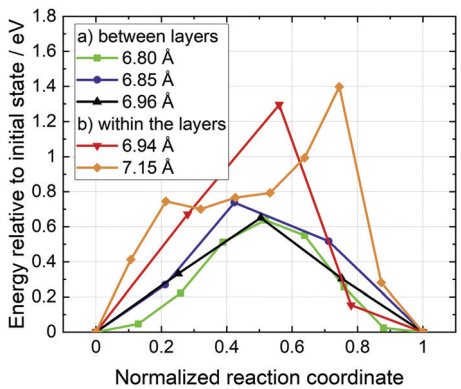

Fig. 2 $CaB_{12}H_{12}$ migration paths. The energy relative to the initial state is shown as a function of the normalized reaction coordinate. Lines are a guide to the eye only.

Between the $B_{12}H_{12}$ layers, Ca migration barriers vary between 640–740 meV with a percolating path having a barrier as low as 650 meV. The latter is to our knowledge one of the lowest reported Ca migration barriers reported for a Ca solid-state electrolyte. Few Ca migration barriers in discharged Ca cathodes (Ca-intercalated materials) have been reported to have lower migration barriers including the hypothetical spinel $CaCr_2O_4$ (610 meV).[28] These materials may be ineligible as solid-state electrolytes due to potential electronic conductivity while for $CaB_{12}H_{12}$ a negligible electronic conductivity is expected due to the calculated band gap larger than 4 eV.

The low barriers in *closo*-borates have been previously attributed to three energy frustration phenomena discussed in detail for $Li_2B_{12}H_{12}$ and $Na_2B_{12}H_{12}$ by Kweon *et al.*[23] Firstly, the high density of accessible interstitial sites leads to several sites of similar energy (frustration of sites). Secondly, cations prefer to dock to specific anion sites, which differ from the sites that lead to a higher preferred symmetry, leading to a local bond frustration. Thirdly, anion reorientations are facile and lead together with other low-frequency thermal vibrations to fluctuations in the local potential ('dynamic frustrations'), leading to a flat energy landscape and facile cation.[23] As the structure of $CaB_{12}H_{12}$ is very similar to the investigated structures ($Li_2B_{12}H_{12}$ and $Na_2B_{12}H_{12}$), we assume that these observations are also true for $CaB_{12}H_{12}$, for which we also show a relatively flat energy landscape in this work (see Fig. 2).

The diffusion coefficient can be approximated as $D = \gamma l^2 \cdot \nu_0 \cdot e^{-\frac{\Delta E_a}{k_B T}}$, where l is the jump distance and γ is the geometrical factor, which includes the number of jump sites n_p and the dimension of diffusion d. The diffusion coefficient then depends on the attempt frequency ν_0 and the migration energy ΔE_a with the Boltzmann constant k_B and the absolute temperature T. For the percolating low migration barrier path for vacancy-mediated diffusion in $CaB_{12}H_{12}$, we can approximate the two-dimensional diffusion with $\gamma = n_p/(2d) = 4/(2.2) = 1$, $l^2 = 4.7 \times 10^{-19}$ m^2 given by the average of the involved migration paths (6.80 Å + 6.96 Å)/2 and an attempt frequency of $\nu_0 = 10^{13}$ s^{-1} (cp. ref. 23) resulting in a diffusion coefficient of 7×10^{-13} cm^2 s^{-1} at 300 K and 9×10^{-11} cm^2 s^{-1} at 373 K. To understand why migration within layers occurs with considerably higher barriers (1300–1400 meV) than between layers (640–740 meV), we investigated several geometric parameters of the two groups of paths. Migration path lengths, coordination environments, bond lengths, polyhedral volumes, and the number of $B_{12}H_{12}$ cages adjacent to the migration path are provided in Table 1 for the migration paths shown in Fig. 1. Ca–H bonds with length, r, <2.7 Å around the mobile Ca in the transition state are considered. Additionally, the effective coordination number according to Hoppe[29] is included. Surprisingly, all of these parameters are similar in both migration path groups despite the migration barriers differing by $\sim$600 meV.

As the geometry of the investigated paths is unable to distinguish between the high and low energy paths, we also investigated the charge density along all paths. To quantify the amount of charge "seen" by the migrating Ca ion, we integrated

Table 1 Geometric parameters of the migration paths. Migration path lengths, coordination environments,[29] bond lengths, polyhedral volumes, and the number of $B_{12}H_{12}$ cages that are adjacent to the migration path are given. Ca–H bonds with length, r, <2.7 Å around the mobile Ca in the transition state are considered

	Migration path between layers	Migration path within the layers
Migration barrier	0.64–0.74 eV	1.30–1.40 eV
Path length	6.8–7.0 Å	6.9–7.2 Å
Coordination	6–7	6
Eff. coordination	6.2, 5.5, 6.0	5.5, 5.5
Ca–H bonds	2.3–2.4 Å	2.3 Å
Polyhedral volume	16–20 Å^3	16 Å^3
Between $B_{12}H_{12}$	2–4	2

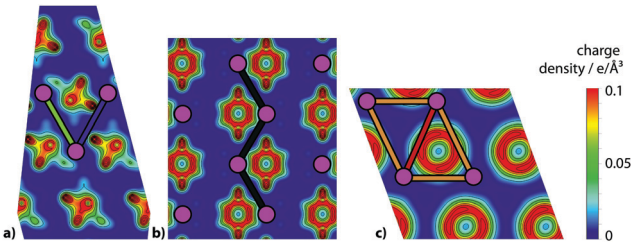

Fig. 3 Charge density of $B_{12}H_{12}$ along all Ca migration paths. Ca positions (pink spheres) are shown in reference to $CaB_{12}H_{12}$. Paths are colored according to the legend in Fig. 1. (a) shows the (−1.55|1.55|1) plane that is a distance of 0.73 Å distance from the origin; (b) is the (1|1|0) plane with 7.37 Å distance from the origin; and (c) is the (0|0|1) plane with 9.38 Å distance from the origin as visualized in Fig. S1 (see ESI†).

the valence electron density in a cylinder with a radius of 0.4 Å that spans between the final and initial site of the migrating Ca. The latter is a new in-house developed method that might provide insights for understanding migration paths in the future. All electron densities were integrated for the Ca-free $B_{12}H_{12}$ framework. Table 2 shows the Ca migration paths lengths, barriers, and their charge density along the path. Fig. 3 and Fig. S2 (see ESI†) show the charge density along all Ca migration paths.

For migration paths between layers, the charge density encountered by the Ca ion is below 0.25 e. For migration paths in the layers, the charge density is 0.49 e or above and, therefore, twice as large. This suggests that Ca needs to move through more charge for migration within the layers than between the layers. The core electrons of Ca^{2+} cannot overlap with the charge density in the structure (Pauli exclusion principle), *i.e.* ion cores repel electron density and must displace the charge density during migration. As a result, an increase in charge encountered along the migration path is counterproductive for migration, indicating why migration between the layers occurs with a smaller activation barrier.

High Ca conductivity requires both low percolating migration barriers as well as a sufficient concentration of Ca vacancies (V''_{Ca}). Therefore, Ca vacancies need to be created in $CaB_{12}H_{12}$. In this work, three ways to create Ca vacancies are investigated: extraction of CaH_2, doping of the B^{3+} sites with C^{4+}, and doping of the Ca^{2+} sites with a number of higher valent (3+ or 4 +) species.

The extraction of CaH_2 creates one Ca and two H vacancies. This concept was experimentally demonstrated by extracting LiH from $Li_2B_{12}H_{12}$ using high energy ball milling to form $Li_{1.92}B_{12}H_{11.69}$.[30] The LiH extraction led to a lattice expansion verified by X-ray diffraction, and Raman experiments showed a local distortion of the B–H bonding. As a result of the Li vacancies created, the conductivity increased by a factor of 1000 according to impedance spectroscopy measurements. Kim *et al.* calculated the extraction of 2% Li ($Li_{64}B_{384}H_{384} \rightarrow Li_{63}B_{384}H_{383} + LiH$) to have a Gibbs free energy of 70 kJ mol^{-1}.[30] In this work, we calculated that 6% Ca extraction ($Ca_{16}B_{192}H_{192} \rightarrow Ca_{15}B_{192}H_{190} + CaH_2$) is highly endothermic, with a reaction enthalpy of 821 kJ mol^{-1} (8.50 eV/V''_{Ca}). Although this approach was used successfully for Li extraction from $Li_2B_{12}H_{12}$, these calculations suggest CaH_2 cannot be readily extracted from $CaB_{12}H_{12}$.

A second way to create Ca vacancies is doping of the B^{3+} sites with C^{4+}, which creates one Ca vacancy per two C dopants. However, the reaction enthalpy for this substitution ($Ca_{16}B_{192}H_{192} + 2\ C \rightarrow Ca_{15}B_{190}C_2H_{192} + 0.5\ Ca + 0.5\ CaB_4$) is highly unfavorable (585 kJ mol^{-1}, 6.06 eV/V''_{Ca}), even in the presence of oxygen ($Ca_{16}B_{192}H_{192} + 2\ C + 0.25\ O_2 \rightarrow Ca_{15}B_{190}C_2H_{192} + 0.5\ CaB_4 + 0.5\ CaO$, 273 kJ mol^{-1}, 2.83 eV/V''_{Ca}), and therefore not practical.

A third way to create Ca vacancies is doping of the Ca^{2+} sites with a higher valent species such as Al^{3+} or rare-earth ions, RE^{3+}. Similar to doping with C^{4+}, one negatively charged Ca vacancy is created per two M^{3+} dopants, *e.g.* in Kröger–Vink notation, $3CaB_{12}H_{12} + 2Al \xrightarrow{CaB_{12}H_{12}} 1V''_{Ca} + 2Al^{\bullet}_{Ca} + 36B^{\times}_{B} + 36H^{\times}_{H} + 3Ca$. In order to investigate if the substitution of one Ca with a higher valent species M^{3+} ($Ca_{13}M_2B_{192}H_{192}$) leads to a stable compound, we calculated the driving force for the decomposition of the doped compound into the lowest energy set of competing compounds (*e.g.* into $CaB_{12}H_{12}$, B_9H_{11}, B and the doping element, see Table S1 in the ESI†). A stable compound has no driving force to separate into a combination of the most stable compounds in its corresponding chemical system,[31] which we determine here using the Materials Project.[32] The driving force for decomposition is calculated as the formation energy of the compound against the convex hull of ground-state energies in the relevant portion of the phase diagram ('energy above the hull per atom', E_{hull}).[33,34] Stable compounds have $E_{hull} < 0$. In Fig. 4, we show the energy per Ca vacancy ($E_{hull} \times 399$) for a number of $Ca_{13}M_2B_{192}H_{192}$ compounds. Elements highlighted in green indicate stable substitutions of a higher valent species for Ca, suggesting they can be used to create

Table 2 Ca migration paths lengths, barriers, and their charge density along the path. The charge density is lower in paths between layers

Path relative to layers	Migration path length [Å]	Migration barrier [eV]	Valence electrons along path [e]
Between	6.80	0.64	0.12
Between	6.85	0.74	0.20
Between	6.96	0.65	0.24
In	6.94	1.30	0.68
In	7.15	1.40	0.49

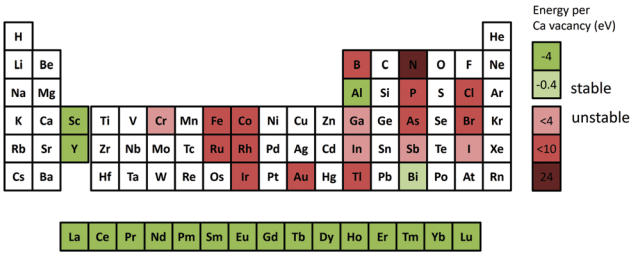

Fig. 4 Energy per Ca vacancy for the structure $Ca_{13}M_2B_{192}H_{192}$ where each candidate dopant ion, M, is shown in green (stable dopant) or red (unstable dopant). Doping $CaB_{12}H_{12}$ with Al, Bi, and rare-earth elements is energetically favorable.

Ca vacancies in $CaB_{12}H_{12}$. $E_{hull} < 0$ provides the equilibrium reaction energy from the neighboring stable entries (inverse distance to the hull). Therefore, doping with aluminum, bismuth, or any of the rare-earth cations is shown to be the most promising way to create Ca vacancies. However, placing a non-mobile ion on the Ca site may also decrease the mobility of Ca. Therefore, a balance between vacancy creation and retention of percolating Ca diffusion pathways is required to optimize the conductivity. As shown in the ESI,† we used Kinetic Monte Carlo simulations to approximate the influence of vacancy creation and retention of percolating Ca diffusion pathways. These simulations show that doping with trivalent cations can increase the Ca ion conductivity by two orders of magnitude at 375 K.

We investigated the mobility of Ca in dodecahydro-*closo*-dodecaborate $CaB_{12}H_{12}$ based on the high mobility of Na and Li in a similar framework. We find that the lowest barrier percolating pathway has a calculated barrier of only 650 meV, which is one of the lowest reported solid-state migration barriers for Ca. Our analysis indicates that the integrated electron density along the path qualitatively correlates with the barrier with a lower electron density leading to a lower barrier. This suggests that the core repulsion of Ca^{2+} with the host's electron density is the prime factor dictating the migration barrier. Our calculations show that doping Ca sites with Al, Bi, or rare-earth elements is a potential low energy way to create the Ca vacancies required to activate the vacancy-mediated diffusion mechanism studied in this work. Although 650 meV is a low barrier for Ca^{2+}, it is still a relatively high barrier for a solid electrolyte, indicating that $CaB_{12}H_{12}$ can probably only be used at high temperature. Possible avenues for improving conductivity are doping with tetravalent ions that decrease migration barriers in their neighborhood or introducing disorder as discussed for $Na_2(B_{12}H_{12})0.5(B_{10}H_{10})_{0.5}$.[35]

Conflicts of interest

There are no conflicts to declare.

Acknowledgements

J. K. and J. X. S. were supported by the Volkswagen group. Phase stability work and doping analysis (CB) were supported by the Joint Center for Energy Storage Research (JCESR). This research used resources of the National Energy Research Scientific Computing Center (NERSC), a U.S. Department of Energy Office of Science User Facility operated under Contract No. DE-AC02-05CH11231. This work used the Extreme Science and Engineering Discovery Environment (XSEDE), which is supported by National Science Foundation grant number ACI-1548562.[36] The authors would like to thank Sebastian Eisele and Steffen Grieshammer for providing technical support and the software for kinetic Monte Carlo simulations MOCASSIN.[37]

References

1 J. Muldoon, C. B. Bucur and T. Gregory, *Chem. Rev.*, 2014, **114**, 11683–11720.
2 N. Kamaya, K. Homma, Y. Yamakawa, M. Hirayama, R. Kanno, M. Yonemura, T. Kamiyama, Y. Kato, S. Hama, K. Kawamoto and A. Mitsui, *Nat. Mater.*, 2011, **10**, 682–686.
3 Y. Seino, T. Ota, K. Takada, A. Hayashi and M. Tatsumisago, *Energy Environ. Sci.*, 2014, **7**, 627–631.
4 T. Famprikis, P. Canepa, J. A. Dawson, M. S. Islam and C. Masquelier, *Nat. Mater.*, 2019, **18**, 1278–1291.
5 A. Ponrouch, C. Frontera, F. Bardé and M. R. Palacín, *Nat. Mater.*, 2016, **15**, 169–172.
6 D. Wang, X. Gao, Y. Chen, L. Jin, C. Kuss and P. G. Bruce, *Nat. Mater.*, 2018, **17**, 16–20.
7 A. L. Lipson, B. Pan, S. H. Lapidus, C. Liao, J. T. Vaughey and B. J. Ingram, *Chem. Mater.*, 2015, **27**, 8442–8447.
8 D. Aurbach, R. Skaletsky and Y. Gofer, *J. Electrochem. Soc.*, 1991, **138**, 3536–3545.
9 P. Canepa, S.-H. Bo, G. Sai Gautam, B. Key, W. D. Richards, T. Shi, Y. Tian, Y. Wang, J. Li and G. Ceder, *Nat. Commun.*, 2017, **8**, 1759.
10 R. Xu, Z. Wu, S. Zhang, X. Wang, Y. Xia, X. Xia, X. Huang and J. Tu, *Chem. – Eur. J.*, 2017, **23**, 13950–13956.
11 J. Koettgen, C. J. Bartel and G. Ceder, *Chem. Commun.*, 2020, **56**, 1952–1955.
12 J. Ni, T. T. Tsai and D. H. Whitmore, *Solid State Ionics*, 1981, **5**, 199–202.
13 A. F. Sammells and B. Schumacher, *J. Electrochem. Soc.*, 1986, **133**, 235–236.
14 S. Fisher, A. Tomich, S. Lovera, J. Kleinsasser, J. Guo, M. Asay, H. Nelson and V. Lavallo, *Chem. Rev.*, 2019, **119**, 8262–8290.
15 R. Mohtadi and S. Orimo, *Nat. Rev. Mater.*, 2017, **2**, 16091.
16 T. J. Udovic, M. Matsuo, A. Unemoto, N. Verdal, V. Stavila, A. V. Skripov, J. J. Rush, H. Takamura and S. Orimo, *Chem. Commun.*, 2014, **50**, 3750–3752.
17 W. S. Tang, A. Unemoto, W. Zhou, V. Stavila, M. Matsuo, H. Wu, S. Orimo and T. J. Udovic, *Energy Environ. Sci.*, 2015, **8**, 3637–3645.
18 W. S. Tang, K. Yoshida, A. V. Soloninin, R. V. Skoryunov, O. A. Babanova, A. V. Skripov, M. Dimitrievska, V. Stavila, S. Orimo and T. J. Udovic, *ACS Energy Lett.*, 2016, **1**, 659–664.

19 W. S. Tang, M. Matsuo, H. Wu, V. Stavila, W. Zhou, A. A. Talin, A. V. Soloninin, R. V. Skoryunov, O. A. Babanova and A. V. Skripov, *et al.*, *Adv. Energy Mater.*, 2016, **6**, 1502237.
20 A. V. Skripov, R. V. Skoryunov, A. V. Soloninin, O. A. Babanova, W. S. Tang, V. Stavila and T. J. Udovic, *J. Phys. Chem. C*, 2015, **119**, 26912–26918.
21 T. J. Udovic, M. Matsuo, W. S. Tang, H. Wu, V. Stavila, A. V. Soloninin, R. V. Skoryunov, O. A. Babanova, A. V. Skripov, J. J. Rush, A. Unemoto, H. Takamura and S. Orimo, *Adv. Mater.*, 2014, **26**, 7622–7626.
22 N. Verdal, T. J. Udovic, V. Stavila, W. S. Tang, J. J. Rush and A. V. Skripov, *J. Phys. Chem. C*, 2014, **118**, 17483–17489.
23 K. E. Kweon, J. B. Varley, P. Shea, N. Adelstein, P. Mehta, T. W. Heo, T. J. Udovic, V. Stavila and B. C. Wood, *Chem. Mater.*, 2017, **29**, 9142–9153.
24 T. J. Carter, R. Mohtadi, T. S. Arthur, F. Mizuno, R. Zhang, S. Shirai and J. W. Kampf, *Angew. Chem., Int. Ed.*, 2014, **53**, 3173–3177.
25 M. N. Guzik, R. Mohtadi and S. Sartori, *J. Mater. Res.*, 2019, **34**, 877–904.
26 V. Stavila, J.-H. Her, W. Zhou, S.-J. Hwang, C. Kim, L. A. M. Ottley and T. J. Udovic, *J. Solid State Chem.*, 2010, **183**, 1133–1140.
27 A. D. Kulkarni, L.-L. Wang, D. D. Johnson, D. S. Sholl and J. K. Johnson, *J. Phys. Chem. C*, 2010, **114**, 14601–14605.
28 M. Liu, Z. Rong, R. Malik, P. Canepa, A. Jain, G. Ceder and K. A. Persson, *Energy Environ. Sci.*, 2015, **8**, 964–974.
29 R. Hoppe, *Z. Kristallogr. - Cryst. Mater.*, 1979, **150**, 23–52.
30 S. Kim, N. Toyama, H. Oguchi, T. Sato, S. Takagi, T. Ikeshoji and S. Orimo, *Chem. Mater.*, 2018, **30**, 386–391.
31 Z. Rong, R. Malik, P. Canepa, G. Sai Gautam, M. Liu, A. Jain, K. Persson and G. Ceder, *Chem. Mater.*, 2015, **27**, 6016–6021.
32 A. Jain, S. P. Ong, G. Hautier, W. Chen, W. D. Richards, S. Dacek, S. Cholia, D. Gunter, D. Skinner, G. Ceder and K. A. Persson, *APL Mater.*, 2013, **1**, 011002.
33 M. Liu, A. Jain, Z. Rong, X. Qu, P. Canepa, R. Malik, G. Ceder and K. A. Persson, *Energy Environ. Sci.*, 2016, **9**, 3201–3209.
34 S. P. Ong, L. Wang, B. Kang and G. Ceder, *Chem. Mater.*, 2008, **20**, 1798–1807.
35 L. Duchêne, S. Lunghammer, T. Burankova, W.-C. Liao, J. P. Embs, C. Copéret, H. M. R. Wilkening, A. Remhof, H. Hagemann and C. Battaglia, *Chem. Mater.*, 2019, **31**, 3449–3460.
36 J. Towns, T. Cockerill, M. Dahan, I. Foster, K. Gaither, A. Grimshaw, V. Hazlewood, S. Lathrop, D. Lifka, G. D. Peterson, R. Roskies, J. R. Scott and N. Wilkins-Diehr, *Comput. Sci. Eng.*, 2014, **16**, 62–74.
37 S. Eisele and S. Grieshammer, *J. Comput. Chem.*, 2020, **31**, 2663–2677.

